

Nonlinear optical microscopy for immunoimaging: a custom optimized system of high-speed, large-area, multicolor imaging

Hui Li^{1,2}, Quan Cui^{1,2}, Zhihong Zhang^{1,2}, Ling Fu^{1,2}, Qingming Luo^{1,2}

¹Wuhan National Laboratory for Optoelectronics-Huazhong University of Science and Technology, Britton Chance Center for Biomedical Photonics, Wuhan 430074, China; ²MoE Key Laboratory for Biomedical Photonics, Department of Biomedical Engineering, Huazhong University of Science and Technology, Wuhan 430074, China

Correspondence to: Ling Fu. Wuhan National Lab for Optoelectronics, Huazhong University of Science and Technology, 1037 Luoyu Road, Wuhan 430074, China. Email: lfu@mail.hust.edu.cn.

Background: The nonlinear optical microscopy has become the current state-of-the-art for intravital imaging. Due to its advantages of high resolution, superior tissue penetration, lower photodamage and photobleaching, as well as intrinsic z-sectioning ability, this technology has been widely applied in immunoimaging for a decade. However, in terms of monitoring immune events in native physiological environment, the conventional nonlinear optical microscope system has to be optimized for live animal imaging. Generally speaking, three crucial capabilities are desired, including high-speed, large-area and multicolor imaging. Among numerous high-speed scanning mechanisms used in nonlinear optical imaging, polygon scanning is not only linearly but also dispersion-freely with high stability and tunable rotation speed, which can overcome disadvantages of multifocal scanning, resonant scanner and acousto-optical deflector (AOD). However, low frame rate, lacking large-area or multicolor imaging ability make current polygonbased nonlinear optical microscopes unable to meet the requirements of immune event monitoring.

Methods: We built up a polygon-based nonlinear optical microscope system which was custom optimized for immunoimaging with high-speed, large-area and multicolor imaging abilities.

Results: Firstly, we validated the imaging performance of the system by standard methods. Then, to demonstrate the ability to monitor immune events, migration of immunocytes observed by the system based on typical immunological models such as lymph node, footpad and dorsal skinfold chamber are shown. Finally, we take an outlook for the possible advance of related technologies such as sample stabilization and optical clearing for more stable and deeper intravital immunoimaging.

Conclusions: This study will be helpful for optimizing nonlinear optical microscope to obtain more comprehensive and accurate information of immune events.

Keywords: Nonlinear optical microscopy; immunoimaging; high-speed; large-area; multicolor

Submitted Oct 15, 2014. Accepted for publication Oct 31, 2014.

doi: 10.3978/j.issn.2223-4292.2014.11.07

View this article at: <http://dx.doi.org/10.3978/j.issn.2223-4292.2014.11.07>

Introduction

The immune system is a network of immune molecules, cells, tissues and organs that work together to defend the organism against attacks from “foreign” invaders. The realization of immunologic function depends on cytokines delivering, cell mobilization, antibody production, *etc.* Each of these processes relies on cell-tissue, cell-cell, and cell-molecule interactions (1-3). Therefore, for immunological studies, intravital imaging methods which can be used to study the location, motility, contact, and interactions of individual cells in three physical dimensions over time are valuable (4). In the field of intravital imaging, the nonlinear optical microscopy based on two-photon absorption and second harmonic generation (SHG) is regarded as the current state-of-the-art (4,5). Due to its advantages of high resolution, superior tissue penetration, lower photodamage and photobleaching, and intrinsic z-sectioning ability (6-8), the technology is widely applied in immunoimaging since 2002 (1,2,9-15).

However, in terms of monitoring immune events in native physiological environment, the conventional nonlinear optical microscope system has to be optimized for live animal studies. Generally speaking, three crucial capabilities are desired, including high-speed, large area and multicolor imaging. Immunocytes migrate and circulate between blood vessels, lymphatic vessels and immune organs to participate in immune events (3). T cells within the lymph node can achieve peak velocities $>25 \mu\text{m}/\text{min}$, and the default trafficking program is analogous to a random walk (9). Leukocytes circulating in blood vessels migrate at a speed of 1-10 mm/s (16). In consideration of the rapidly migration of cells within thick tissues, volume sampling should be less than 20 s to avoid blurring (2). Thus, high-speed imaging is essential to provide an accurate readout of instantaneous velocities from multidimensional $[x, y, z, \text{time } (t)]$ data sets (10,17). High-resolution large-area imaging can avoid cell escaping out of the observation volume during long-term monitoring (10,17), and allows the visualization of cell-cell, and cell-molecule interactions within proper context of surrounding tissue environment (5). Multicolor imaging allows simultaneous observation of differently labeled cell types, molecules and surrounding environment like vessels, connective tissues, *etc.* (10).

The imaging speed of a microscope system is largely decided by the laser scanning mechanism (5). With high precision positioning, good scanning resolution, and high compactness at reasonable costs, galvanometer scanner

driven by a linear saw-tooth control signal is one of the most commonly used scanning devices (18-21). However, the scanning speed, ranging from 0.5 to 2 frames per second (f/s), limits its application in intravital imaging systems (22). In order to acquire faster frame rate, various high-speed scanning mechanisms are incorporated into nonlinear optical microscopes. Among them, multifocal scanning imaging (23,24) and devices like resonant scanner, acousto-optical deflector (AOD) (25), and polygonal mirror (26) are commonly used. Due to limited dose of each excitation beam to the specimen, multifocal imaging has the advantages of slow photobleaching and low photodamage (27,28). Nevertheless, the interference between adjacent foci due to scattering could lead to decreased sectioning ability (27,29,30). Besides, the introduction of optical multiplexers could lead to low utilization efficiency of the laser power as well as decreased fluorescence collection efficiency. Moreover, to create multiple foci with enough energy for fluorescence excitation, higher laser power is required. In terms of resonant scanner, due to image distortion caused by the sinusoidal dependence of the position with time, data acquisition is complicated by introducing image correction or nonuniform pixel clock (31). Besides, the constant resonant frequency limits its flexibility in imaging speed adjustment (32). For AOD, since it can cause significant dispersion of ultra-short pulses and introduce spherical aberration, the imaging system is fairly complicated by laser pulse width and shape compensation modules (33-36). Another high-speed scanner is polygon which scans not only linearly but also dispersion-freely with high stability and tunable rotation speed, thereby, overcomes disadvantages of resonant scanner and AOD. However, existing nonlinear optical microscopes based on polygon scanning are generally not custom optimized for immunoimaging. A frame rate lower than 30 f/s, the lacking of large-area imaging ability or insufficient fluorescence detection channels (1-2 colors), make them unable to meet the requirements of immune event monitoring (5,37-41).

In this study, we reported a polygonal mirror based nonlinear optical microscope system which was custom optimized for immunoimaging. The system has a frame rate ranging from 5 to 82 f/s depending on image dimension and the rotation speed of the polygonal mirror. At the same time, it has capabilities of large-area and multicolor imaging based on a precise-controlled three-dimensional (3-D) translation subsystem and a four-channel fluorescence or SHG detection module, respectively. Besides, to solve the common problem of fluorescent crosstalk between

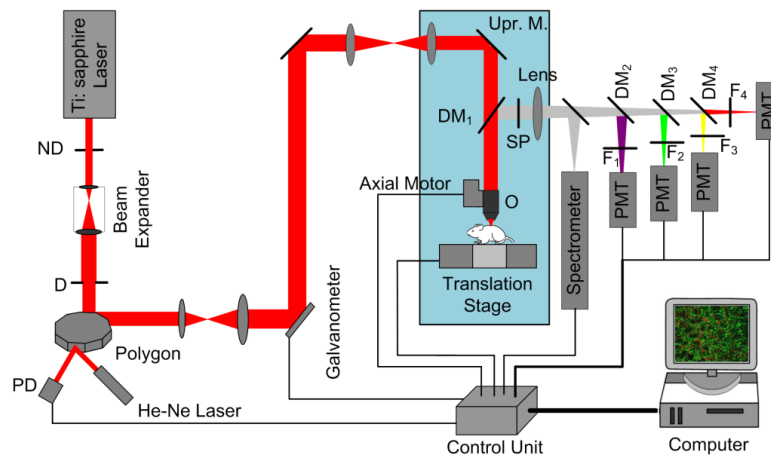


Figure 1 Schematic of the high-speed, large-area, multicolor nonlinear optical microscope system. ND, neutral density filter; D, diaphragm; PD, photodiode detector; DM, dichroic mirror; O, objective lens; SP, short-pass filter; F, band-pass filter; PMT, photomultiplier tube; Upr. M., upright microscope.

different channels caused by the emission spectra overlap of fluorescent proteins or dyes in multicolor imaging, a spectrum detection channel is incorporated into the system to provide reference spectra used for further spectra unmixing (42). We validated the performance of the system by standard methods and demonstrated its ability of monitoring immune events by imaging typical immunological models including lymph node, footpad and dorsal skinfold chamber. The results indicate that, our high-speed, large-area, multicolor, nonlinear optical microscope system is expert in tracking immune dynamics in native physiological environment. Based on the system, more comprehensive and accurate information of immune events can be derived.

Materials and methods

Imaging system

The schematic of the high-speed, large-area, multicolor nonlinear optical microscope system is shown in *Figure 1*. A Ti:Sapphire laser (Maitai BB, Spectra-Physics) is used as the excitation source (pulse duration: ~ 100 fs, repetition rate: 80 MHz and tunable range: 710 to 980 nm). By two different types of scanners, the expanded laser beam is rapidly raster scanned across a sample plane. A gold-coated 36-faceted polygon (DT-36-250-020, Lincoln Laser) accomplishes the high-speed horizontal scanning (x axis) and a galvanometric mirror with a bandwidth of 2 kHz (6215H, Cambridge Technology) performs the slow vertical scanning (y axis). The spinning polygon deflects the laser beam repetitively

by its serial facets, such that unidirectionally scans a line 36 times per rotation with a specific angular range. There are four selections for the rotation speed of the polygon: 10K, 20K, 40K and 54.945K r/min (rotation per minute). The two lenses between the scanners function together as a relay element to project the excitation beam deflected by the polygon onto the center of the galvanometric mirror.

In order to facilitate live animal imaging, an upright microscope (BX51WI, Olympus) with a modified epiluminescence light path is incorporated into this imaging system. The scanning beam is coupled into the microscope by another group of relay lenses. After passing through a dichroic mirror (FF735-Di01-25 \times 36, Semrock), the beam is focused on the specimen by an objective, typically XLPLN25XWMP, Olympus. The induced multiphoton fluorescence and SHG signals are collected by the same objective. This objective is optimized for nonlinear optical microscopy imaging. Furthermore, as a result of low magnification, 25 \times , high NA, 1.05, and long working distance, 2 mm, large field of view (FOV), high spatial resolution, flexible and deep intravital imaging can be simultaneously obtained via the objective. To perform large-volume imaging, a translation stage (H117, Prior Scientific) with resolution of 40 nm and travel range of 114 mm \times 76 mm is used for xy -plane large-area scan, while an axial motor mounted on the objective focus knob (Prior Scientific) with resolution of 2 nm is used for z -axial scan.

After split from the excitation laser by the dichroic mirror above and passing through a short-pass filter (FF01-750/SP-25, Semrock) to remove residual scattered light,

the emission light enters into the detection module. A beamsplitter (BS80/20, Olympus) separates the emission light into two beams by a ratio of 2:8. 20% of the light is detected by a spectrometer (ARC-SP2356, Princeton Instruments) for emission spectrum analysis, while 80% of that is separated into four beams by three dichroic mirrors (generally, we choose one of the two combinations: FF409-Di01-25×36, FF510-Di01-25×36 and FF562-Di02-25×36; or FF510-Di01-25×36, FF562-Di02-25×36 and FF605-Di01-25×36, Semrock) and enters different multiphoton fluorescence or SHG detection channels to accomplish multicolor imaging. Each channel includes a band-pass filter (Semrock) and a photomultiplier tube (PMT, H7422A-40, Hamamatsu) to record emission light of specific waveband. The signals collected by PMTs are amplified, and then acquired by a high-speed data acquisition system for image reconstruction, display and storage. The core of the data acquisition system is a FlexRIO FPGA module (PXIe-7962R, National Instruments), cooperating with a data streaming system (HDD-8265, National Instruments).

A separate He-Ne laser illuminating the polygon facet along with a photodiode (PDA-50, Thorlabs) detecting its reflection is used to encode the position of the polygon. The output signal from the photodiode detection is converted to TTL levels by a custom-built circuit board. Since each TTL pulse corresponds to a fixed position within the line scanned by one polygon facet, it is used as the horizontal synchronization signal. Based on this signal, the x , y scanning, xy -plane sample translation, z -axis objective translation and data acquisition are synchronized by custom-designed LabView (National Instruments) program. The y -axis scanning and data acquisition are both triggered by the TTL pulse and stops after a whole FOV plane is scanned. Then the acquired data is reconstructed to a frame of image, and further displayed and stored. Afterwards, the xy -plane translation stage steps to the next area or the z -axis objective motor steps to the next plane. By repeating these steps, serial images are obtained to reconstruct a tissue volume. 3-D time-lapse imaging can be further accomplished by scanning the tissue volume repeatedly.

Mice

Actb-EGFP C57BL/6 mice were obtained from Dr. Zhiying He (Second Military Medical University, Shanghai, China). CX3CR1-GFP C57BL/6 mice and B6.Cg-Tg(Itagx-Venus)1Mnz/J mice were purchased from Jackson Laboratory (Bar Harbor, Maine, USA). All cell types in

Actb-EGFP C57BL/6 mice express EGFP. Most of the CX3CR1-GFP cells were monocytes (~90%). All Itagx-Venus cells are dendritic cells (DCs). These transgenic mice were reproduced in the specific pathogen-free (SPF) animal facility of Britton Chance Center for Biomedical Photonics, Wuhan National Laboratory for Optoelectronics-Huazhong University of Science and Technology (Wuhan, China). Lymphocytes and neutrophils used for tail-vein injection were obtained from C57BL/6 mice purchased from Shanghai Slaccas Laboratory Animal Co., Ltd. (Hunan, China), and respectively stained with CMTMR dye and eFluor670 dye afterwards. All mice experiments were performed according to the animal experiment guidelines of the Animal Experimentation Ethics Committee of HUST.

Data processing

Serial images of one sample plane were combined into a large-area image section by a custom-designed MATLAB (The MathWorks) program. The cell migrating trajectories were obtained by tracking time-lapse imaging videos using Image-Pro Plus (Media Cybernetics). 3-D reconstruction of tissue volume was done by Imaris (Bitplane).

Results

Performance of the imaging system

To evaluate if the imaging system meets the requirements of immunoimaging, we tested its performance including spatial resolution, FOV, imaging speed, as well as the ability for multicolor fluorescence and spectrum detection by standard methods.

All of the imaging results shown in this paper were obtained by the 25× NA1.05 water immersion objective (XLPLN25XWMP, Olympus). By using FITC labeled fluorescent beads with a diameter of 200 nm (Invitrogen), we measured the lateral and axial resolution of this objective at the excitation wavelength of 800 nm, which are around 0.49 and 1.65 μm (theoretically 0.30 and 0.97 μm), respectively (Figure 2). Spatial resolution on this level is sufficient for subcellular immunoimaging. In addition, the FOV of the objective is measured by imaging fluorescent beads with a diameter of 10.4 μm (Spherotech), which is around 300 μm × 500 μm (theoretically 800 μm × 800 μm). The imaging area can be expanded by large-area imaging based on sample translation.

The imaging speed of the system is largely decided by

the high-speed horizontal scanner, polygon. In addition, for 3-D imaging, the response time and travel speed of the sample translation stage and axial objective motor should also be taken into consideration. Corresponding to the four selections of the polygon rotation speed, the calculated frame rates of single-FOV x, y, t imaging of the system are 15, 30, 60 and 82 f/s for image size of 396 pixel \times 240 pixel, while 5, 10, 20 and 27 f/s for image size of 1,188 pixel \times 720 pixel. The number of lines per image was set to be an integer multiple of the number of polygon facets, 36, to ensure that the same facet scans the same line of the reconstructed image on every successive frame, so that possible vertical scrolling effects introduced in the image by slight discrepancies between the facets can be avoided (5). The measured speeds were well consistent with the calculated values. In order to ensure that sufficient excitation photons can be acquired during each pixel time, we generally choose 30 f/s (polygon

rotation speed of 20K r/min with image size of 240 pixel \times 396 pixel) to achieve a compromise between imaging speed and quality. In this case, the speed of single-FOV x, y, z, t imaging is 6 f/s and large-area x, y, t imaging is 10 f/s. Thus, the imaging of a tissue volume of 300 $\mu\text{m} \times$ 500 $\mu\text{m} \times$ 50 μm with 2- μm z spacing can be finished within \sim 4.2 s, which is much lesser than the 20-s-volume-sampling requirement for immunoinaging to avoid blurring (2). In addition, imaging of an area of 2 mm \times 2 mm, which is generally enough to observe the tumor microenvironment or the whole lymph node, can be finished within \sim 3 s. Generally speaking, the imaging system has provided a sufficiently fast imaging speed which not only allows tracking rapidly migrating immunocytes within the 3-D tissue environment, but also allows repeatedly scanning of the same area for multi-frame averaging to improve image quality.

To test the ability of the imaging system for multicolor fluorescence detection, mixed fluorescent beads (diameter, 10.4 μm , Spherotech) with four colors (ultraviolet, yellow, Nile red and purple) are used for imaging. As shown in *Figure 3*, beads labeled with different dyes can be easily distinguished. Furthermore, the rhodamine B solution with a concentration of 1.5×10^{-2} g/L is used to test the spectrum detection ability of the system. The measured emission spectrum with a central wavelength of 584 nm is shown in *Figure 4* (excitation wavelength, 780 nm), which is well consistent with the previous study (43). The four-channel fluorescence detection module allows simultaneously observing cell-cell or cell-molecular interactions within native physiological environment including extracellular matrix and vessels. Actually, using these four channels, at most $15 (2^n - 1, n \text{ is the number of detection channels})$

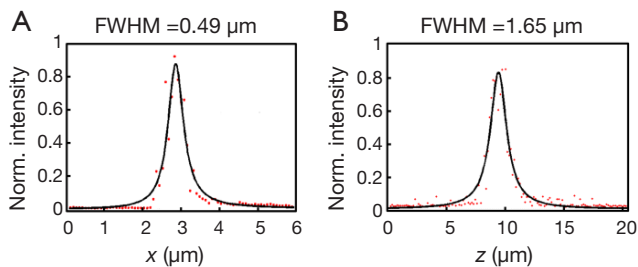


Figure 2 The lateral (A) and axial (B) resolution of the high-speed, large-area, multicolor nonlinear optical microscope measured using fluorescent beads (diameter, 200 nm). Red dots: experimental data; Black solid lines: Gaussian fit. FWHM, full width at the half maximum.

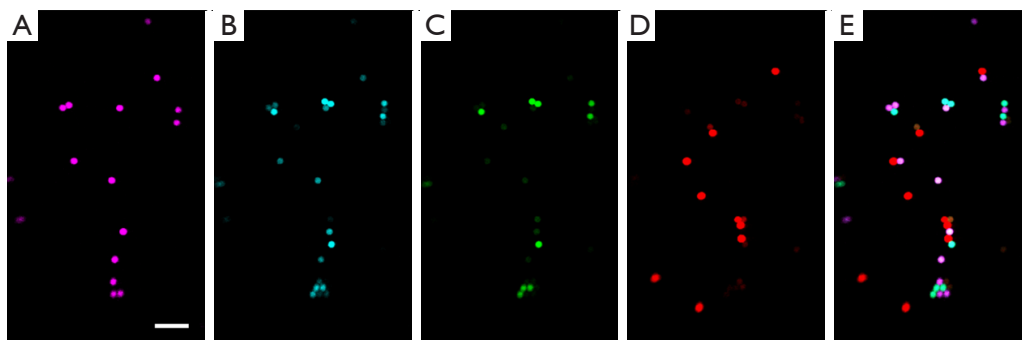


Figure 3 Multicolor imaging of mixed fluorescent beads (diameter, 10.4 μm) with four colors: ultraviolet, yellow, Nile red and purple. Four channels separated by dichroic mirrors (Semrock), FF409-Di01-25 \times 36, FF510-Di01-25 \times 36 and FF562-Di02-25 \times 36, as well as respectively mounted with filters (Semrock), 390/40 nm (A), 485/20 nm (B), 525/40 nm (C) and 600/14 nm (D) are used for fluorescence detection. (E) merged image of A-D. Scale bar, 50 μm .

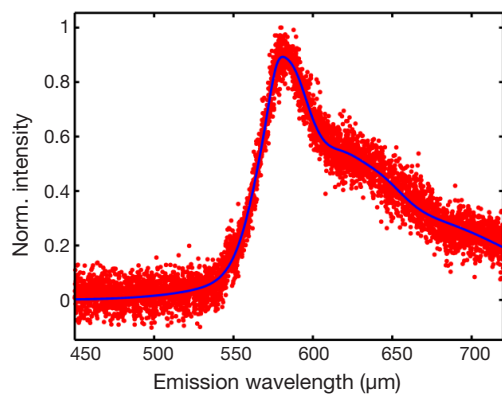


Figure 4 The measured fluorescence emission spectrum of rhodamine B.

populations can be separately distinguished based on binary determinations of the presence of a dye (9). Besides, the spectrum detection channel can provide the emission spectrum information of samples, which can be used as reference for spectra unmixing in multicolor imaging (42).

Ability of the imaging system to monitor immune events

To demonstrate the capability of the imaging system for immune events monitoring, we imaged typical immunological models including lymph node, footpad and dorsal skinfold chamber. Representative results are shown in *Figures 5-8*.

Lymph nodes are secondary lymphoid organs. They strategically locate throughout the body to trap and present foreign antigens from peripheral tissues to prime the adaptive immune response, so that they are ideal for studies of immune cell interactions (44). *Figure 5* shows the large-area imaging results of the popliteal lymph node explanted in phosphate buffered saline (PBS) which has been picked from Actb-EGFP mouse. The imaging area is 1 mm × 3 mm. Cells expressing EGFP are shown, mainly consisting of lymphocytes. Further, lymphocyte motility within the popliteal lymph node is shown in *Figure 6*. The lymph node was picked from Actb-EGFP mouse with tail-vein injected lymphocytes, and then explanted in PBS for imaging. Migrating EGFP⁺ host lymphocytes (green), injected lymphocytes labeled with CMTMR dye (red) and collagen fibers (blue) indicated by SHG signals can be simultaneously observed. Typical lymphocyte migrating trajectories are indicated by white lines (*Figure 6B-I*). It can be observed that, lymphocytes within lymph node

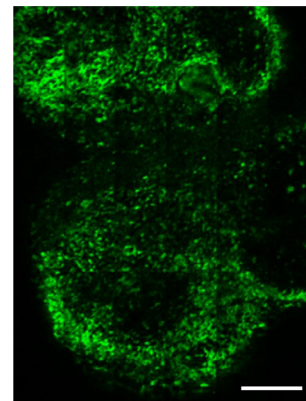


Figure 5 Large-area imaging of the popliteal lymph node of Actb-EGFP mouse. Cells expressing EGFP are shown, mainly consisting of lymphocytes. The excitation wavelength is 880 nm. The average laser power on the sample surface is ~30 mW. The channel with a filter of 525/40 nm (Semrock) is used for fluorescence detection. Scale bar, 200 µm. EGFP, enhanced green fluorescent protein.

characteristically move in a consistent direction for short periods, while crawl in an amoeboid-manner over longer times, which is consistent with previous studies (11).

The mouse footpad is a classical immunological model site for studies of delayed type hypersensitivity (DTH) reaction. Since it is easy to fix and access, it has become an ideal site for long-term noninvasive intravital optical imaging in immunology (45). *Figure 7* shows the intravital motility of monocytes/macrophages (MMs) and neutrophils in the inflammatory foci of the DTH reaction occurring at the mouse footpad. The DTH reaction was elicited by aggregated ovalbumin. Since neutrophils and MMs play important roles in the development of the DTH reaction (45), neutrophils labeled with eFluor670 dye were tail-vein injected into the CX3CR1-GFP mouse which contains EGFP⁺ MMs, for simultaneously observation. The detailed description of the footpad model of DTH reaction can be found in the work of Meijie Luo, *et al.* (45). As shown in *Figure 7B-I*, MMs (green) and neutrophils (red) migrating within 3-D native physiological environment (extracellular matrix is shown as blue) at the early stage of DTH reaction (4 h post-challenge) can be observed. White lines indicate their typical migrating trajectories. The results demonstrate that MMs and neutrophils almost migrate directionally with approximately same velocity at the early stage of DTH reaction.

The dorsal skinfold chamber has been commonly used for intravital microscopy in studies of tumors. It allows

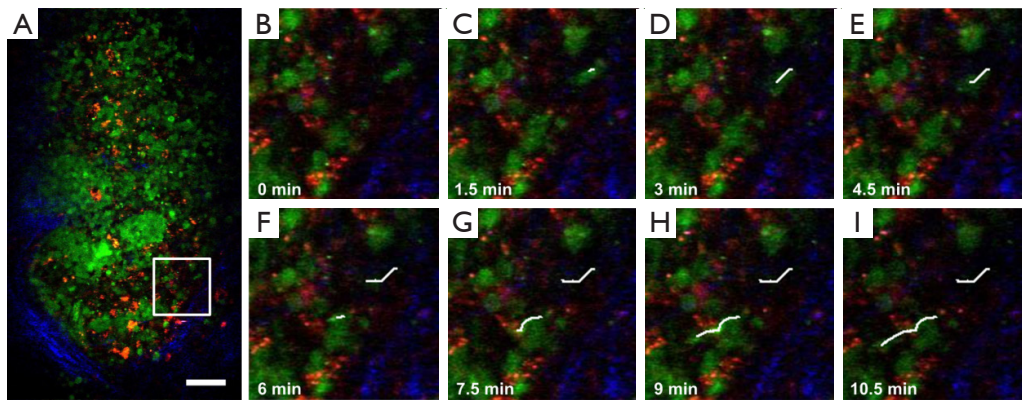


Figure 6 Time-lapse imaging of lymphocyte motility within the popliteal lymph node of Actb-EGFP transgenic mouse with tail-vein injected lymphocytes. B-I are magnified views of the area marked in A. Green: EGFP+ host lymphocytes; Red: injected lymphocytes labeled with CMTMR dye; Blue: collagen fibers indicated by second harmonic generation (SHG) signals. White lines indicate cell migrating trajectories. The excitation wavelength is 900 nm. The average laser power on the sample surface is ~20 mW. Three channels separated by dichroic mirrors (Semrock), FF510-Di01-25×36 and FF562-Di01-25×36, as well as respectively mounted with filters (Semrock), 452/45 nm (SHG), 520/28 nm (EGFP) and 575/15 nm (CMTMR) are used for detection. Scale bar, 50 μ m.

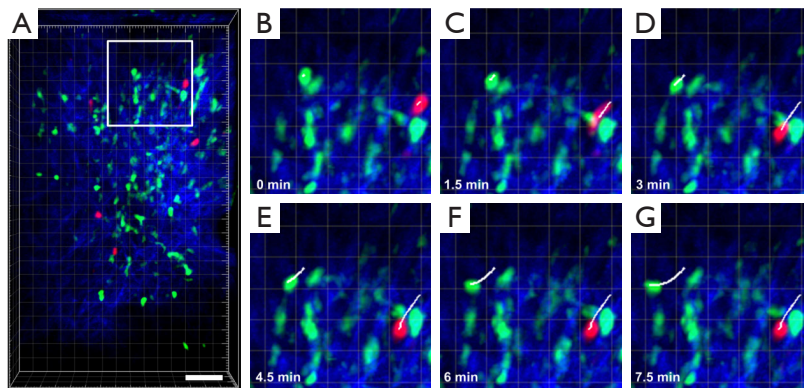


Figure 7 3-D intravital imaging of the motility of monocytes/macrophages (MMs) and neutrophils in the inflammatory foci of the delayed type hypersensitivity reaction occurring at the footpad of CX3CR1-GFP transgenic mouse at 4 h post-challenge. B-G are magnified views of the area marked in A. Green: EGFP+ host MMs; Red: tail-vein injected neutrophils labeled with eFluor670 dye; Blue: collagen fibers indicated by second harmonic generation (SHG) signals. White lines indicate cell migrating trajectories. The excitation wavelength is 900 nm. The average laser power on the sample surface is ~20 mW. Three of the four channels separated by dichroic mirrors (Semrock), FF510-Di01-25×36, FF562-Di01-25×36 and FF605-Di01-25×36, as well as respectively mounted with filters (Semrock), 452/45 nm (SHG), 525/40 nm (EGFP) and 647/57 nm (eFluor670) are used for detection. Imaging depth, 60 μ m. Scale bar, 50 μ m.

long-term observation of tumor growth and the changes occurring in the tumor microenvironment at different cancer stages. *Figure 8* shows the *in vivo* migration of DCs within the mouse dorsal skinfold chamber. The extension and retraction of pseudopodia and the amoeboid-manner crawling of DCs can be easily tracked. Further quantitative analysis on the migration behaviors of these immunocytes could provide new clues to studies of tumor immune response. Thereby, new strategies for the diagnosis and

treatment of tumors might be developed.

Generally speaking, the results have demonstrated that, the imaging system performs well in immune events monitoring based on typical immunological models such as lymph node, footpad and dorsal skinfold chamber.

Discussion and conclusions

In conclusion, we built up a nonlinear optical microscope

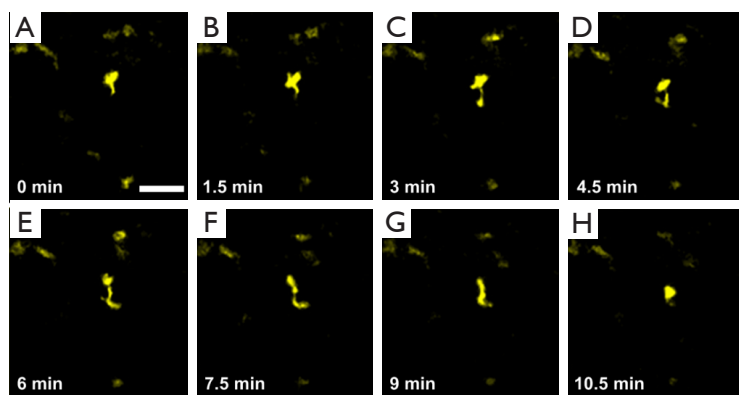


Figure 8 Intravital imaging of the motility of dendritic cells within dorsal skinfold chamber of B6.Cg-Tg(Itagx-Venus)1Mnz/J transgenic mouse. The excitation wavelength is 880 nm. The average laser power on the sample surface is ~18 mW. The channel with a filter of 543/22 nm (Semrock) is used for fluorescence detection. Scale bar, 30 μ m.

system for immunoimaging, which was custom optimized for high-speed, large-area, multicolor imaging. The system has a frame rate ranging from 5 to 82 f/s. The imaging of a tissue volume of 300 μ m \times 500 μ m \times 50 μ m with 2- μ m z spacing can be finished within ~4.2 s, while the imaging of an area enough to observe the tumor microenvironment or the whole lymph node, 2 mm \times 2 mm, can be finished within ~3 s. The four fluorescence or SHG detection channels of the system can separately distinguish at most 15 populations based on binary determinations of the presence of a dye. Beside, a spectrum detection channel is incorporated to provide reference spectra for spectra unmixing in multicolor imaging. The measured parameters such as spatial resolution, FOV, imaging speed, *etc.* as well as the imaging results of typical immunological models including lymph node, footpad and dorsal skinfold chamber, have all demonstrated that, the imaging system meets the requirements of immunoimaging and performs well in immune events monitoring.

However, the optimizing of intravital immunoimaging is not only dependent on the imaging system, but also dependent on the sample preparation. There are three critical problems affecting the image quality of intravital immunoimaging, which can be improved by proper sample stabilization and process. First, the subject motion caused by the cardiac contractions, pulsatile blood flow, and significant overall movements during the inhalation/exhalation cycle of the live animal, usually leads to mismatch of adjacent image frames, making it difficult to do further quantitative analysis (16). Second, the imaging sites of *in vivo* investigations are usually irregular and difficult to access, such as lymph node, tumor, *etc.* To reduce subject motion and facilitate optical

access, a series of custom-designed chambers, holders or flexible detection front-end, as well as image registration and correction algorithms are developed for intravital imaging of the tumor, lymph node, footpad, lung, skin and eye (5,16,44-46). Third, although near-infrared excitation light used in nonlinear optical imaging has reduced the absorption of light by living tissues, the scattering still limits the imaging depth to ~100 μ m. To extend imaging depth, various optical clearing technics have been developed for deeper *in vivo* imaging, but limited to skin applications (47). Advanced optical clearing technologies which can be widely used for living tissues exposed by minimally invasive surgery are expected to improve the immunoimaging depth.

Therefore, by combining chambers or holders custom-designed for different imaging sites, and using advanced optical clearing technics to process the tissue, more stable and deeper imaging will be obtained by our home-built nonlinear optical microscope system in intravital immunoimaging.

Acknowledgements

This work was supported by the National Major Scientific Research Program of China (Grant No. 2011CB910401), and National Natural Science Foundation of China (No. 61178077). We thank Shuhong Qi, Meijie Luo, Lili Zhou and Zheng Liu for sample preparation. We also thank the Optical Bioimaging Core Facility of WNLO-HUST for the support in data acquisition, and the Analytical and Testing Center of HUST for spectral measurements.

Disclosure: The authors declare no conflict of interest.

References

- Cahalan MD, Parker I. Choreography of cell motility and interaction dynamics imaged by two-photon microscopy in lymphoid organs. *Annu Rev Immunol* 2008;26:585-626.
- Germain RN, Robey EA, Cahalan MD. A decade of imaging cellular motility and interaction dynamics in the immune system. *Science* 2012;336:1676-81.
- Alitalo K. The lymphatic vasculature in disease. *Nat Med* 2011;17:1371-80.
- Pittet MJ, Weissleder R. Intravital imaging. *Cell* 2011;147:983-91.
- Veilleux I, Spencer JA, Biss DP, Côté D. In vivo cell tracking with video rate multimodality laser scanning microscopy. *IEEE J Sel Top Quantum Electron* 2008;14:10-8.
- Meyer T, Schmitt M, Dietzek B, Popp J. Accumulating advantages, reducing limitations: multimodal nonlinear imaging in biomedical sciences - the synergy of multiple contrast mechanisms. *J Biophotonics* 2013;6:887-904.
- Hu W, Zhao G, Wang C, Zhang J, Fu L. Nonlinear optical microscopy for histology of fresh normal and cancerous pancreatic tissues. *PLoS One* 2012;7:e37962.
- Li H, Feng C, Chen Z, Yang Y, Jiang W, Zhuo S, Zhu X, Guan G, Chen J. Distinguishing Between Hyperplastic and Adenomatous Polyps and Normal Colonic Mucosa By Using Multiphoton Laser Scanning Microscopy. *J Innov Opt Health Sci* 2014;7:1350056. Available online: <http://www.worldscientific.com/doi/abs/10.1142/S1793545813500569>
- Miller MJ, Wei SH, Cahalan MD, Parker I. Autonomous T cell trafficking examined in vivo with intravital two-photon microscopy. *Proc Natl Acad Sci U S A* 2003;100:2604-9.
- Bullen A, Friedman RS, Krummel MF. Two-photon imaging of the immune system: a custom technology platform for high-speed, multicolor tissue imaging of immune responses. *Curr Top Microbiol Immunol* 2009;334:1-29.
- Miller MJ, Wei SH, Parker I, Cahalan MD. Two-photon imaging of lymphocyte motility and antigen response in intact lymph node. *Science* 2002;296:1869-73.
- Bousso P, Bhakta NR, Lewis RS, Robey E. Dynamics of thymocyte-stromal cell interactions visualized by two-photon microscopy. *Science* 2002;296:1876-80.
- Stutzmann GE, Parker I. Dynamic multiphoton imaging: a live view from cells to systems. *Physiology (Bethesda)* 2005;20:15-21.
- Germain RN, Miller MJ, Dustin ML, Nussenzweig MC. Dynamic imaging of the immune system: progress, pitfalls and promise. *Nat Rev Immunol* 2006;6:497-507.
- Cahalan MD, Parker I, Wei SH, Miller MJ. Two-photon tissue imaging: seeing the immune system in a fresh light. *Nat Rev Immunol* 2002;2:872-80.
- Looney MR, Thornton EE, Sen D, Lamm WJ, Glenn RW, Krummel MF. Stabilized imaging of immune surveillance in the mouse lung. *Nat Methods* 2011;8:91-6.
- Matheu MP, Cahalan MD, Parker I. Immunoinaging: studying immune system dynamics using two-photon microscopy. *Cold Spring Harb Protoc* 2011;2011:pdb.top99.
- Montagu J. Scanners—galvanometric and resonant. In: Driggers RG, Hoffman C, Driggers R. eds. *Encyclopedia of Optical Engineering*. Marcel Dekker, New York, 2003:2465-87.
- Marshall GF. *Handbook of Optical and Laser Scanning*. Marcel Dekker, New York, 2004.
- Hua D, Qi S, Li H, Zhang Z, Fu L. Monitoring the process of pulmonary melanoma metastasis using large area and label-free nonlinear optical microscopy. *J Biomed Opt* 2012;17:066002.
- Chong SP, Lai T, Zhou Y, Tang S. Tri-modal microscopy with multiphoton and optical coherence microscopy/tomography for multi-scale and multi-contrast imaging. *Biomed Opt Express* 2013;4:1584-94.
- Larson JM, Schwartz, SA, Davidson MW. Resonant scanning in laser confocal microscopy. Available online: <http://www.microscopyu.com/articles/confocal/resonantscanning.html>
- Cha JW, Tzeranis D, Subramanian J, Yannas IV, Nedivi E, So PT. Spectral-resolved multifocal multiphoton microscopy with multianode photomultiplier tubes. *Opt Express* 2014;22:21368-81.
- Liu L, Qian J, Li Y, Peng X, Yin J. Monte Carlo Simulation of Multifocal Stochastic Scanning System. *J Innov Opt Health Sci* 2014;7:1350054.
- Shao Y, Qin W, Liu H, Qu J, Peng X, Niu H, Gao BZ. Ultrafast, large-field multiphoton microscopy based on an acousto-optic deflector and a spatial light modulator. *Opt Lett* 2012;37:2532-4.
- Duma VF. Scanning in biomedical imaging: from classical devices to handheld heads and micro-systems. *Proc SPIE* 2014;8925:8925 0L.
- Egner A, Andresen V, Hell SW. Comparison of the axial resolution of practical Nipkow-disk confocal fluorescence microscopy with that of multifocal multiphoton microscopy: theory and experiment. *J Microsc*

- 2002;206:24-32.
28. Straub M, Lodemann P, Holroyd P, Jahn R, Hell SW. Live cell imaging by multifocal multiphoton microscopy. *Eur J Cell Biol* 2000;79:726-34.
 29. Sheetz KE, Hoover EE, Carriles R, Kleinfeld D, Squier JA. Advancing multifocal nonlinear microscopy: development and application of a novel multibeam Yb:KGd(WO₄)₂ oscillator. *Opt Express* 2008;16:17574-84.
 30. Fricke M, Nielsen T. Two-dimensional imaging without scanning by multifocal multiphoton microscopy. *Appl Opt* 2005;44:2984-8.
 31. Sanderson MJ. Acquisition of multiple real-time images for laser scanning microscopy mirrors. *Microsc Anal* 2004;18:2-6.
 32. Aylward RP. The advances & technologies of galvanometer-based optical scanners. Part of the SPIE Conference on Optical Scanning: Design and Application 1999;3787:158-64. Available online: <http://proceedings.spiedigitallibrary.org/ConferenceProceedings.aspx>
 33. Kim KH, Buehler C, Bahlmann K, Ragan T, Lee WC, Nedivi E, Heffer EL, Fantini S, So PT. Multifocal multiphoton microscopy based on multianode photomultiplier tubes. *Opt Express* 2007;15:11658-78.
 34. Iyer V, Losavio BE, Saggau P. Compensation of spatial and temporal dispersion for acousto-optic multiphoton laser-scanning microscopy. *J Biomed Opt* 2003;8:460-71.
 35. Reddy GD, Saggau P. Fast three-dimensional laser scanning scheme using acousto-optic deflectors. *J Biomed Opt* 2005;10:064038.
 36. Zeng S, Lv X, Zhan C, Chen WR, Xiong W, Jacques SL, Luo Q. Simultaneous compensation for spatial and temporal dispersion of acousto-optical deflectors for two-dimensional scanning with a single prism. *Opt Lett* 2006;31:1091-3.
 37. Kim KH, Ragan T, Previte MJ, Bahlmann K, Harley BA, Wiktor-Brown DM, Stitt MS, Hendricks CA, Almeida KH, Engelward BP, So PT. Three-dimensional tissue cytometer based on high-speed multiphoton microscopy. *Cytometry A* 2007;71:991-1002.
 38. Ragan T, Sylvan JD, Kim KH, Huang H, Bahlmann K, Lee RT, So PT. High-resolution whole organ imaging using two-photon tissue cytometry. *J Biomed Opt* 2007;12:014015.
 39. Kim KH, Buehler C, So PT. High-speed, two-photon scanning microscope. *Appl Opt* 1999;38:6004-9.
 40. Kim P, Puoris'haag M, Côté D, Lin CP, Yun SH. In vivo confocal and multiphoton microendoscopy. *J Biomed Opt* 2008;13:010501.
 41. Biss DP, Sumorok D, Burns SA, Webb RH, Zhou Y, Bifano TG, Côté D, Veilleux I, Zamiri P, Lin CP. In vivo fluorescent imaging of the mouse retina using adaptive optics. *Opt Lett* 2007;32:659-61.
 42. Zimmermann T. Spectral imaging and linear unmixing in light microscopy. *Adv Biochem Eng Biotechnol* 2005;95:245-65.
 43. Emission spectrum of Rhodamine B. Available online: <http://omlc.org/spectra/PhotochemCAD/html/009.html>
 44. Liou HL, Myers JT, Barkauskas DS, Huang AY. Intravital imaging of the mouse popliteal lymph node. *J Vis Exp* 2012;(60). pii: 3720.
 45. Luo M, Zhang Z, Li H, Qiao S, Liu Z, Fu L, Shen G, Luo Q. Multi-scale optical imaging of the delayed type hypersensitivity reaction attenuated by rapamycin. *Theranostics* 2014;4:201-14.
 46. Sellers SL, Payne GW. Intravital microscopy of the inguinal lymph node. *J Vis Exp* 2011;(50). pii: 2551.
 47. Zhu D, Wen X, Wang J. Advances in optical clearing of skin in vivo. *SPIE Newsroom* 2011;10.1117/2.1201103.003567.

Cite this article as: Li H, Cui Q, Zhang Z, Fu L, Luo Q. Nonlinear optical microscopy for immunoimaging: a custom optimized system of high-speed, large-area, multicolor imaging. *Quant Imaging Med Surg* 2015;5(1):30-39. doi: 10.3978/j.issn.2223-4292.2014.11.07